



An Explicit Adaptive Finite Difference Method for the Cahn–Hilliard Equation

Seokjun Ham¹ · Yibao Li² · Darae Jeong³ · Chaeyoung Lee¹ · Soobin Kwak¹ · Youngjin Hwang¹ · Junseok Kim¹

Received: 16 March 2022 / Accepted: 25 August 2022 / Published online: 5 September 2022

© The Author(s), under exclusive licence to Springer Science+Business Media, LLC, part of Springer Nature 2022

Abstract

In this study, we propose an explicit adaptive finite difference method (FDM) for the Cahn–Hilliard (CH) equation which describes the process of phase separation. The CH equation has been successfully utilized to model and simulate diverse field applications such as complex interfacial fluid flows and materials science. To numerically solve the CH equation fast and efficiently, we use the FDM and time-adaptive narrow-band domain. For the adaptive grid, we define a narrow-band domain including the interfacial transition layer of the phase field based on an undivided finite difference and solve the numerical scheme on the narrow-band domain. The proposed numerical scheme is based on an alternating direction explicit (ADE) method. To make the scheme conservative, we apply a mass correction algorithm after each temporal iteration step. To demonstrate the superior performance of the proposed adaptive FDM for the CH equation, we present two- and three-dimensional numerical experiments and compare them with those of other previous methods.

Keywords Adaptive finite difference scheme · Stable numerical method · Cahn–Hilliard equation

Mathematics Subject Classification 65M50 · 65M06 · 35G20

Communicated by David Nicholls.

✉ Junseok Kim
cfdkim@korea.ac.kr

¹ Department of Mathematics, Korea University, Seoul 02841, Republic of Korea

² School of Mathematics and Statistics, Xi'an Jiaotong University, Xi'an 710049, China

³ Department of Mathematics, Kangwon National University, Gangwon-do 24341, Republic of Korea

1 Introduction

The Cahn–Hilliard (CH) equation represents the dynamics of spinodal decomposition that occurs when a single thermodynamic phase spontaneously separates into two phases (Cahn and Hilliard 1958; Grant 1993):

$$\frac{\partial \phi(\mathbf{x}, t)}{\partial t} = \Delta \left[F'(\phi(\mathbf{x}, t)) - \epsilon^2 \Delta \phi(\mathbf{x}, t) \right], \quad (1)$$

where $\phi(\mathbf{x}, t)$ is a phase field at space $\mathbf{x} \in \Omega$ and time t , ϵ is a positive constant, and $F(\phi) = (\phi^2 - 1)^2/4$. The boundary condition is the homogeneous Neumann boundary condition: $\mathbf{n} \cdot \nabla \phi(\mathbf{x}, t) = 0$ and $\mathbf{n} \cdot \nabla \Delta \phi(\mathbf{x}, t) = 0$ for $\mathbf{x} \in \partial\Omega$, where \mathbf{n} is the outer unit normal vector. Because the CH equation can efficiently handle topological changes, it has been widely studied and applied in various applications. However, because the CH equation is a fourth-order nonlinear partial differential equation (PDE), the explicit time discretization requires a very small time step for stability. In order to overcome the strict time step constraints, various semi-implicit (Zhu et al. 1999; Li and Qiao 2017; Li et al. 2016, 2021) and implicit (Benešová et al. 2014; Bosch et al. 2014; Xu et al. 2019) schemes have been proposed to solve the CH equation with good numerical stability. Splitting-type numerical schemes have been used for variable studies (Chen et al. 2012; Li et al. 2018; Cheng et al. 2019; Chen et al. 2020; Meng et al. 2020; Hao 2021) with energy stability. Several different methods have been utilized to numerically solve the CH equation. Zhai et al. (2021) proposed a novel high-order linearly operator splitting method for the nonlocal viscous CH equation with the spectral deferred correction method. Their method can avoid the nonlinear iteration and obtain high temporal accuracy. Feng et al. (2020) considered the CH equation with an imposed advection term. They studied the effects of the imposed advection on phase separation of the CH equation. Ainsworth and Mao (2017) investigated the fractional CH equation with fractional free energy. They presented well-posedness and several numerical examples of the fractional CH equation. Li et al. (2016a) used the phase-field model to the minimized CH dynamics. Mohammadi and Dehghan (2019) presented an adaptive time algorithm for the CH equation. Fu and Han (2021) used a finite element method (FEM) to overcome the challenges of solving the CH equation with a degenerate mobility function. Theljani et al. (2020) proposed the image inpainting method which solves the CH equation on an adaptive mesh. Figure 1 shows an adaptive mesh (Theljani et al. 2020).

Chen et al. (2016) solved the CH-type diffusion equation and the Navier–Stokes equation using a space-time adaptive finite difference method. Isotropic and strongly anisotropic CH systems were solved using the multigrid method on an adaptive grid (Chen et al. 2018). Figure 2a and b shows the adaptive meshes (Chen et al. 2016, 2018) for two- and three-dimensional spaces, respectively.

Compared to the unstructured methods, the adaptive mesh refinement (AMR) framework can provide spatial multi-resolution (Berger and Oliger 1984), which imposes a good choice for the large-scale simulation with challenging physical issues (Li et al. 2016b; Zhou and Xie 2021). There are many applications for the AMR algorithm, i.e., crystal growth (Li and Kim 2012, 2017), thin film (Li et al. 2014; Sun et al.

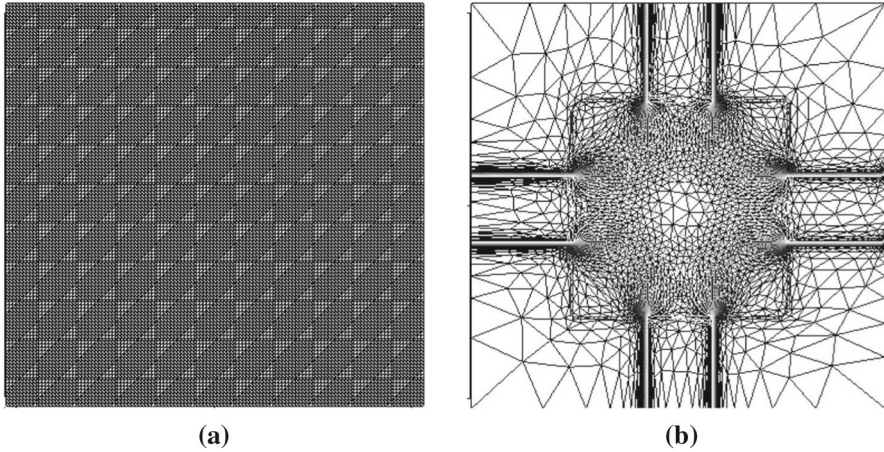


Fig. 1 **a** Uniform mesh and **b** adaptive mesh. Reprinted from (Theljani et al. 2020) with permission from SAGE Publishing

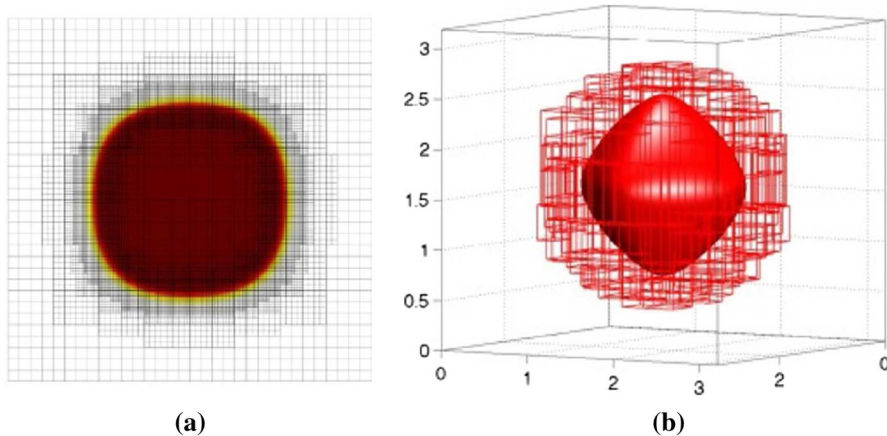


Fig. 2 **a** and **b** are 2D and 3D adaptive meshes, reprinted from (Chen et al. 2016) and (Chen et al. 2018) with permission from Elsevier, respectively

2007), nonlinear wave (Dohnal and Uecker 2016), and computational fluid dynamics (Berger and Colella 1989). Koliesnikova et al. (2021) proposed a hierarchical mesh refinement scheme driven by a posteriori error estimator. Li et al. (2021) proposed an implicitly discretized surface method with an AMR method. To overcome the difficulties of imposing the boundary conditions by considering the skin depth, Jung and Yoo (2021) used an AMR framework for microwave applications of metallic structures. Grave and Coutinho (2021) used a PDE model to investigate the dynamics of COVID-19 using an AMR method. Their model can represent various spatial scales.

Kay and Welford (2006) presented a multigrid FEM for the CH equation. Banas and Nürnberg (2008) presented an AMR method for the CH equation. Ceniceros and Rom (2007) presented a nonstiff, fully AMR method for the CH equation. Wise et al.

(2007) presented a second-order accurate and adaptive FDM to solve the CH equation in 2D and 3D spaces. Stogner et al. (2008) proposed a variational formulation and C^1 FEM with an AMR method. The fourth-order spatial accurate compact schemes were developed for the CH equation in 2D (Lee et al. 2014) and 3D (Li et al. 2016c) spaces. The above-mentioned methods are based on a semi-implicit splitting or implicit scheme, in which a multigrid method or other numerical solvers should be performed on coarse and fine grid levels. Therefore, the explicit AMR-based method is much simpler to implement.

The main purpose of this study is to present an explicit adaptive FDM for the CH equation. The primary advantage of the proposed method is its simplicity compared to existing adaptive numerical schemes for the CH equation which use complex data structure and implicit solvers.

The outline of this article is as follows. In Sect. 2, the proposed numerical method is described. In Sect. 3, we present several computational experiments to confirm the superior performance of the proposed explicit AMR method. We conclude this paper in Sect. 4.

2 Numerical Method

We describe the proposed numerical solution algorithms on the adaptive domain for the 2D and 3D CH equations using the Saul'yev scheme (Yang et al. 2022) and adaptive methodology (Jeong et al. 2021).

2.1 Two-Dimensional Algorithm

For the completeness of exposition, we briefly describe the explicit finite difference scheme for the CH equation in the 2D domain $\Omega = (L_x, R_x) \times (L_y, R_y)$. For more details, see (Yang et al. 2022). Let $\Omega_h = \{(x_i = L_x + h(i - 0.5), y_j = L_y + h(j - 0.5)) | i = 1, \dots, N_x, j = 1, \dots, N_y\}$, where the spatial space step is $h = (R_x - L_x)/N_x = (R_y - L_y)/N_y$. Here, N_x and N_y are the numbers of the grid points. Let $\phi_{ij}^n = \phi(x_i, y_j, n\Delta t)$, where Δt is the time step for a nonnegative integer n . First, we discretize Eq. (1) using the linear convex splitting scheme (Li et al. 2017):

$$\frac{\phi_{ij}^{n+1} - \phi_{ij}^n}{\Delta t} = \Delta_d((\phi_{ij}^n)^3 - 3\phi_{ij}^n) + 2\Delta_d\phi_{ij}^{n+1} - \epsilon^2\Delta_d^2\phi_{ij}^{n+1}, \quad (2)$$

where $\Delta_d\phi_{ij} = (\phi_{i+1,j} + \phi_{i-1,j} - 4\phi_{ij} + \phi_{i,j+1} + \phi_{i,j-1})/h^2$ and $\Delta_d^2\phi_{ij} = \Delta_d(\Delta_d\phi_{ij})$. We define a temporary narrow domain as

$$\Omega_{\text{tmp}}^n = \{(x_i, y_j) | |\nabla\phi_{ij}^n| > \xi, 1 \leq i \leq N_x, 1 \leq j \leq N_y\}, \quad (3)$$

where ξ is a parameter and

$$\nabla\phi_{ij}^n = \left(\frac{\phi_{i+1,j}^n - \phi_{i-1,j}^n}{2h}, \frac{\phi_{i,j+1}^n - \phi_{i,j-1}^n}{2h} \right).$$

A space-time adaptive narrow-band domain Ω_{nb}^n is defined using Ω_{tmp}^n :

$$\Omega_{nb}^n = \bigcup_{p=-m}^{p=m} \bigcup_{q=-m}^{q=m} \{(x_{i+p}, y_{j+q}) | (x_i, y_j) \in \Omega_{tmp}^n\} \tag{4}$$

for some positive integer m , which makes buffer points. We can control the narrow-band domain by adjusting ξ and m values appropriately. We define doubly layered exterior boundary points of Ω_{nb}^n as

$$\Omega_{bd}^n = \bigcup_{p=-2}^{p=2} \bigcup_{q=-2}^{q=2} \{(x_{i+p}, y_{j+q}) | (x_i, y_j) \in \Omega_{nb}^n\} \setminus \Omega_{nb}^n.$$

For better understanding of the narrow-band domain construction, let us consider the following circular shape at time $t = n\Delta t$:

$$\phi(x, y, t) = \tanh\left(\frac{30 - \sqrt{x^2 + y^2}}{\sqrt{2}\epsilon}\right), \tag{5}$$

which is shown in Fig. 3a and the red line is the contour of ϕ at zero level. Figure 3b, c, and d shows $|\nabla\phi^n|$ with $z = \xi$ -plane, temporary domain Ω_{tmp}^n , and space-time adaptive narrow-band domain Ω_{nb}^n (closed circle) with the exterior boundary points Ω_{bd}^n (open circle), respectively. We use the values defined at Ω_{bd}^n for the exterior boundary values when we solve Eq. (6) on the interior boundary points. Then, using the Saul'yev method (Yang et al. 2022), we have the following updating scheme: For $j = 1, 2, \dots, N_y$, for $i = 1, 2, \dots, N_x$. If $(x_i, y_j) \in \Omega_{nb}$, then

$$\begin{aligned} \phi_{ij}^{n+1} = & \frac{1}{r} \left[\frac{\phi_{ij}^n}{\Delta t} + \Delta_d((\phi_{ij}^n)^3 - 3\phi_{ij}^n) + \frac{2}{h^2} (\phi_{i+1,j}^n + \phi_{i-1,j}^{n+1} - 2\phi_{ij}^n \right. \\ & + \phi_{i,j+1}^n + \phi_{i,j-1}^{n+1}) - \frac{\epsilon^2}{h^4} \{ \phi_{i+2,j}^n + \phi_{i-2,j}^{n+1} + \phi_{i,j+2}^n + \phi_{i,j-2}^{n+1} \\ & + 2(\phi_{i+1,j+1}^n + \phi_{i+1,j-1}^n + \phi_{i-1,j+1}^n + \phi_{i-1,j-1}^{n+1}) \\ & \left. - 8(\phi_{i+1,j}^n + \phi_{i-1,j}^{n+1} + \phi_{i,j+1}^n + \phi_{i,j-1}^{n+1}) + 10\phi_{ij}^n \right], \tag{6} \end{aligned}$$

where $r = 1/\Delta t + 4/h^2 + 10\epsilon^2/h^4$. The other 7 ‘for loop’ cases are similarly defined. Next, we adopt the adaptive methodology, which was developed for the Allen–Cahn equation, see (Jeong et al. 2021).

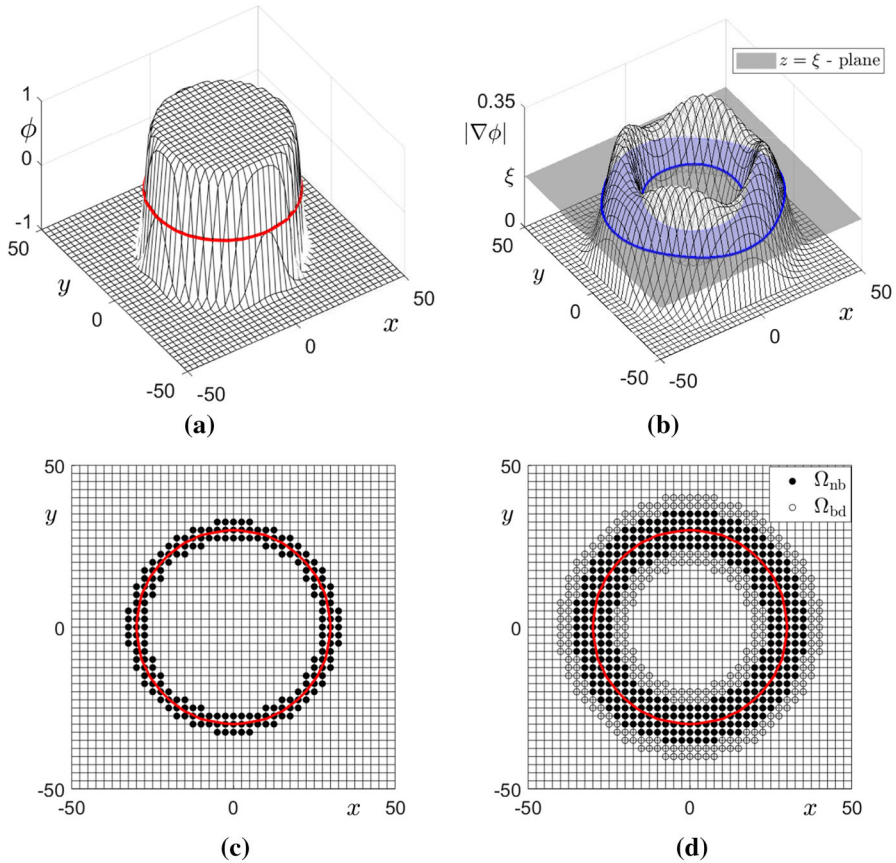


Fig. 3 Schematic illustration for Ω_{tmp}^n , Ω_{nb}^n and Ω_{bd}^n : **a** mesh plot of ϕ with the zero level contour (red line), **b** $|\nabla\phi^n|$ and $z = \xi$ -plane, **c** temporary domain Ω_{tmp}^n , and **d** space-time adaptive narrow-band domain Ω_{nb}^n (closed circle) with the exterior boundary points Ω_{bd}^n (open circle) (Color figure online)

Because the Saul’yev-type scheme is generally not conservative, we adopt a mass correction step (Jeong et al. 2020):

$$\phi_{ij}^{n+1} = \phi_{ij}^{n+1} + \frac{\sum_{(x_p, y_q) \in \Omega_{\text{nb}}^n} (\phi_{pq}^n - \phi_{pq}^{n+1})}{\sum_{(x_p, y_q) \in \Omega_{\text{nb}}^n} \sqrt{F(\phi_{pq}^{n+1})}} \sqrt{F(\phi_{ij}^{n+1})} \text{ for } (x_i, y_j) \in \Omega_{\text{nb}}^n. \quad (7)$$

We should note that the mass correction is only done on the narrow-band domain because the values of ϕ outside the narrow-band domain are unchanged.

Remark 1 Solving problems using the FDM in adaptive meshes is very complex and difficult; nevertheless, there are studies that have presented new numerical ideas and convincing numerical results on this interesting scientific problem (Feng et al. 2018; Wise et al. 2011). However, because most adaptive methods have very com-

plex relational expressions, numerical methods have been verified through numerical experiments rather than analytically verified.

2.2 Three-Dimensional Algorithm

The 3D numerical solution algorithm and adaptive grid generation are straightforward extension of the 2D ones. Let $\Omega = (L_x, R_x) \times (L_y, R_y) \times (L_z, R_z)$. Let $\Omega_h = \{(x_i = L_x + h(i - 0.5), y_j = L_y + h(j - 0.5), z_k = L_z + h(k - 0.5)) | i = 1, \dots, N_x, j = 1, \dots, N_y, k = 1, \dots, N_z\}$ be the discrete domain, where $h = (R_x - L_x)/N_x = (R_y - L_y)/N_y = (R_z - L_z)/N_z$. Here, N_x, N_y and N_z are the numbers of the grid points. Let $\phi_{ijk}^n = \phi(x_i, y_j, z_k, n\Delta t)$. We start with the following method (Li et al. 2017):

$$\frac{\phi_{ijk}^{n+1} - \phi_{ijk}^n}{\Delta t} = \Delta_d((\phi_{ijk}^n)^3 - 3\phi_{ijk}^n) + 2\Delta_d\phi_{ijk}^{n+1} - \epsilon^2\Delta_d^2\phi_{ijk}^{n+1}, \tag{8}$$

where $\Delta_d\phi_{ijk} = (\phi_{i+1,j,k} + \phi_{i-1,j,k} + \phi_{i,j+1,k} + \phi_{i,j-1,k} + \phi_{i,j,k+1} + \phi_{i,j,k-1} - 6\phi_{ijk})/h^2$ and $\Delta_d^2\phi_{ijk} = \Delta_d(\Delta_d\phi_{ijk})$. Then, using the Saul'yev method (Yang et al. 2022), we have the following updating scheme:

For $i = 1, 2, \dots, N_x$, for $j = 1, 2, \dots, N_y$, for $k = 1, 2, \dots, N_z$, (9)

If $(x_i, y_j, z_k) \in \Omega_{nb}$, then

$$\begin{aligned} \phi_{ijk}^{n+1} = & \frac{1}{r} \left[\frac{\phi_{ijk}^n}{\Delta t} + \Delta_d((\phi_{ijk}^n)^3 - 3\phi_{ijk}^n) + \frac{2}{h^2}(\phi_{i+1,j,k}^n + \phi_{i-1,j,k}^{n+1} + \phi_{i,j+1,k}^n \right. \\ & + \phi_{i,j-1,k}^{n+1} + \phi_{i,j,k+1}^n + \phi_{i,j,k-1}^{n+1} - 3\phi_{ijk}^n) - \frac{\epsilon^2}{h^4} \{ \phi_{i+2,j,k}^n + \phi_{i-2,j,k}^{n+1} \\ & + \phi_{i,j+2,k}^n + \phi_{i,j-2,k}^{n+1} + \phi_{i,j,k+2}^n + \phi_{i,j,k-2}^{n+1} + 2(\phi_{i+1,j+1,k}^n + \phi_{i+1,j-1,k}^{n+1} \\ & + \phi_{i+1,j,k+1}^n + \phi_{i+1,j,k-1}^{n+1} + \phi_{i-1,j+1,k}^n + \phi_{i-1,j-1,k}^{n+1} + \phi_{i-1,j,k+1}^n \\ & + \phi_{i-1,j,k-1}^{n+1} + \phi_{i,j+1,k+1}^n + \phi_{i,j+1,k-1}^{n+1} + \phi_{i,j-1,k+1}^n + \phi_{i,j-1,k-1}^{n+1} \\ & \left. - 12(\phi_{i+1,j,k}^n + \phi_{i-1,j,k}^{n+1} + \phi_{i,j+1,k}^n + \phi_{i,j-1,k}^{n+1} + \phi_{i,j,k+1}^n + \phi_{i,j,k-1}^{n+1}) \right], \tag{10} \end{aligned}$$

where $r = 1/\Delta t + 6/h^2 + 21\epsilon^2/h^4$. The other 47 ‘for loop’ cases are similarly defined. A space-time adaptive narrow-band domain Ω_{nb}^n is defined as $\Omega_{nb}^n = \{(x_i, y_j, z_k) | |\nabla\phi_{ijk}^n| > \xi, 1 \leq i \leq N_x, 1 \leq j \leq N_y, 1 \leq k \leq N_z\}$, where

$$\nabla\phi_{ijk}^n = \left(\frac{\phi_{i+1,j,k}^n - \phi_{i-1,j,k}^n}{2h}, \frac{\phi_{i,j+1,k}^n - \phi_{i,j-1,k}^n}{2h}, \frac{\phi_{i,j,k+1}^n - \phi_{i,j,k-1}^n}{2h} \right). \tag{11}$$

Figure 4 illustrates a schematic of narrow-band domain on 3D space. It shows the temporal evolution of Ω_{nb}^n (dots) with isosurface of solutions at zero level.

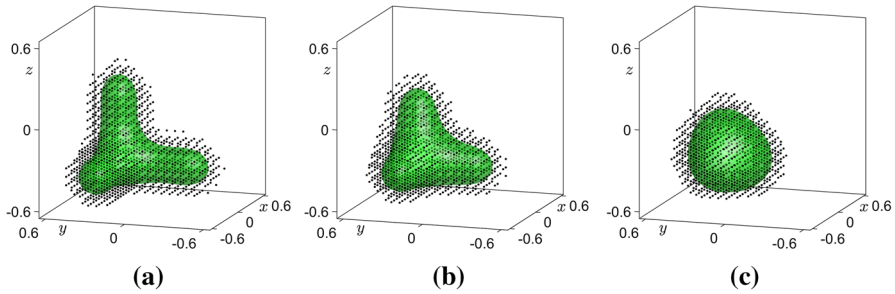


Fig. 4 a–c Snapshots of the temporal evolution of narrow-band domain Ω_{nb}^n (dots) in 3D space

To make the numerical scheme conservative, we apply the mass correction algorithm after each temporal iteration:

$$\phi_{ijk}^{n+1} = \phi_{ijk}^{n+1} + \frac{\sum_{(x_p, y_q, z_r) \in \Omega_{nb}^n} (\phi_{pqr}^n - \phi_{pqr}^{n+1})}{\sum_{(x_p, y_q, z_r) \in \Omega_{nb}^n} \sqrt{F(\phi_{pqr}^{n+1})}} \sqrt{F(\phi_{ijk}^{n+1})} \text{ for } (x_i, y_j, z_k) \in \Omega_{nb}^n. \tag{12}$$

In Eqs. (2) and (8), we only considered a first-order linear convex splitting scheme. It can be extended to second-order linear convex splitting schemes (Guo et al. 2016, 2021; Chen et al. 2019; Dong et al. 2020). For example, we may use the following second-order method (Guo et al. 2016): for given $\phi_{ijk}^{n-1}, \phi_{ijk}^n \in \Omega_h$,

$$\frac{\phi_{ijk}^{n+1} - \phi_{ijk}^n}{\Delta t} = \Delta_d \mu_{ijk}^{n+\frac{1}{2}}, \tag{13}$$

where

$$\mu_{ijk}^{n+\frac{1}{2}} = \Delta_d \left(\chi(\phi_{ijk}^{n+1}, \phi_{ijk}^n) - \phi_{ijk}^{n+\frac{1}{2}} - \epsilon^2 \Delta_d \hat{\phi}_{ijk}^{n+\frac{1}{2}} \right), \tag{14}$$

$$\chi(\phi_{ijk}^{n+1}, \phi_{ijk}^n) = \frac{1}{4}(\phi_{ijk}^{n+1} + \phi_{ijk}^n) \left[(\phi_{ijk}^{n+1})^2 + (\phi_{ijk}^n)^2 \right], \tag{15}$$

$$\phi_{ijk}^{n+\frac{1}{2}} = \frac{3}{2}\phi_{ijk}^n - \frac{1}{2}\phi_{ijk}^{n-1}, \quad \hat{\phi}_{ijk}^{n+\frac{1}{2}} = \frac{3}{4}\phi_{ijk}^{n+1} + \frac{1}{4}\phi_{ijk}^{n-1}. \tag{16}$$

3 Computational Tests

We perform various computational simulations using the proposed numerical solution algorithm on 2D and 3D spaces. Through the computational experiments, we demonstrate the efficiency and accuracy of our proposed numerical solution algorithm. For numerical simulations, we define the interface layer parameter ϵ_l as follows (Jeong et al. 2021):

$$\epsilon_l = \frac{lh}{2\sqrt{2} \tanh^{-1}(0.9)}, \tag{17}$$

where l is a positive integer. Unless otherwise stated, numerical experiments are performed in $\Omega = (-1, 1)^d$ ($d = 2, 3$) with grid points $N_x = N_y = N_z = 128$, uniform spatial step $h = 2/N_x = 2/N_y = 2/N_z$, and $\epsilon = \epsilon_4$.

3.1 Stability Test

In this section, we test the time step stability of the proposed adaptive method. In 2D and 3D spaces, we consider square and cubic shapes as initial conditions, respectively. We define a maximum time step Δt_{max} , which is a numerical maximum time step that guarantees the non-blow-up of the numerical solutions. The condition under which the numerical solution blows up is defined when $\max_{i \in I} \{\phi(\mathbf{x}_i, 100\Delta t)\} > 1.7$, where I is the index set of grid points. In 2D and 3D computational domains $\Omega = (0, 1)^d$, where d is dimension, the given initial conditions are as follows:

$$\phi(x, y, 0) = \begin{cases} +1, & \text{if } 0.25 < x < 0.75, 0.25 < y < 0.75, \\ -1, & \text{otherwise,} \end{cases} \tag{18}$$

and

$$\phi(x, y, z, 0) = \begin{cases} +1, & \text{if } 0.25 < x < 0.75, 0.25 < y < 0.75, 0.25 < z < 0.75, \\ -1, & \text{otherwise,} \end{cases} \tag{19}$$

respectively. Tables 1 and 2 list the maximum time step Δt_{max} in 2D and 3D space, respectively, with three different spatial grid sizes $h = 1/64, 1/128$, and $1/256$. The stability test confirms that the proposed adaptive method can use sufficiently large time steps for the stable numerical solutions.

3.2 Two-Dimensional Space

In 2D space, we compare solutions of the entire domain with those of adaptive domains and investigate effects of the parameters m, ξ , and K which generate the adaptive domain.

Table 1 Stability test results in 2D space

Case	Δt_{max}
$h = 1/64$	$8.8199\text{e-}4 \approx 14790h^4$
$h = 1/128$	$2.2140\text{e-}4 \approx 59432h^4$
$h = 1/256$	$5.6189\text{e-}5 \approx 241330h^4$

Table 2 Stability test results in 3D space

Case	Δt_{max}
$h = 1/64$	$1.1704e-4 \approx 1964h^4$
$h = 1/128$	$6.3239e-5 \approx 16976h^4$
$h = 1/256$	$1.5285e-5 \approx 65650h^4$

In Fig. 5, we observe the temporal evolution with the following square shape initial condition,

$$\phi(x, y, 0) = \begin{cases} +1, & \text{if } -0.5 < x < 0.5, \quad -0.5 < y < 0.5, \\ -1, & \text{otherwise,} \end{cases} \quad (20)$$

We compare the solutions of the CH equation computed on the entire domain (solid line) with the adaptive domain (solid line with markers). The solutions on the adaptive domain fit well with the solutions on the entire domains. For efficient computations, buffer size m which adjusts the narrow-band domain should be appropriately controlled. To find a proper the buffer size m , we investigate the evolution of the solutions on the adaptive narrow-band domain according to the value of m . In Fig. 6, we experiment with a square spiral shape. As a result of Fig. 6, $m = 6$ is sufficient to accurately represent the solution of the CH equation.

To compare CPU times for the entire domains with those for adaptive domains, we define a period K of updating the adaptive domain at every K time steps. That is, we update the computational domain Ω_{nb}^n when $n = Kp$ for $p = 0, 1, 2, \dots$, where K is a positive integer. In Fig. 7, we show the comparison results for entire and adaptive domains. The CH equation is solved on a rectangular domain $\Omega = (-1, 1) \times (-0.5, 0.5)$ with parameter values: $N_x = 128, N_y = 64, \Delta t = h^2, m = 4$, and $\xi = 0.5$. We investigate the dynamics until the solution of the CH equation becomes circular from the rectangular initial condition. Figure 7a shows CPU times for entire and adaptive domains. It shows that as K increases, the CPU times decrease.

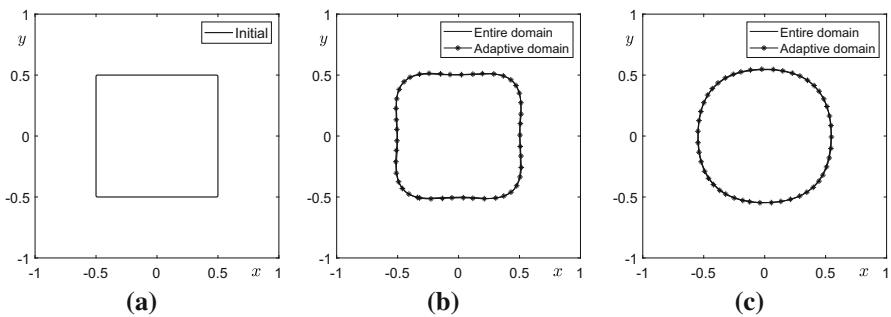


Fig. 5 Temporal evolution of the contours of ϕ at zero level with square initial condition. **a–c** are snapshots of solution for entire and adaptive domains at $t = 0, t = 9000\Delta t$, and $t = 30000\Delta t$, respectively. Here, $m = 6, \Delta t = 0.1h^2$, and $\xi = 0.5$ are used

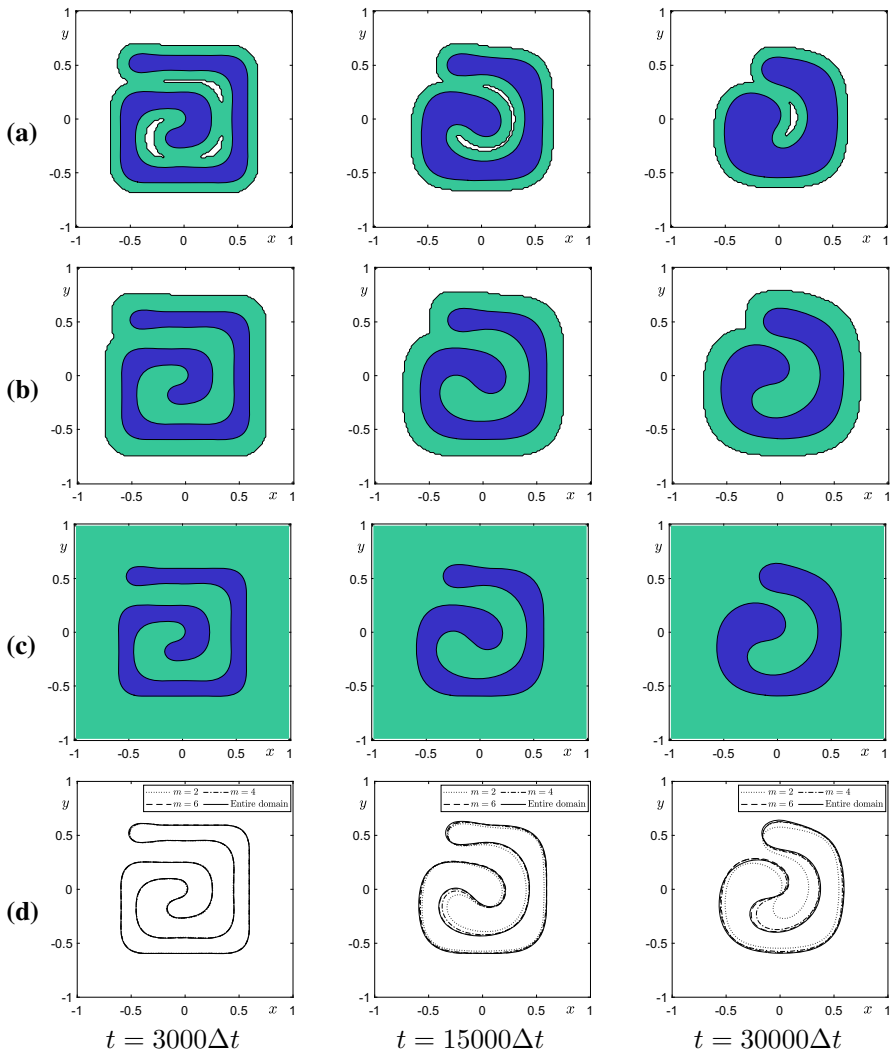


Fig. 6 Snapshots of solution and narrow-band domain for **a–b** adaptive domain $m = 2$ and $m = 6$, **c** entire domain. **d** Overlapped contour of solutions at zero level. Left to right column, $t = 3000\Delta t$, $t = 15000\Delta t$, and $t = 30000\Delta t$. Here, $\xi = 0.5$ and $\Delta t = 0.1h^2$ are used

Figure 7b shows contours of ϕ at zero for the entire and adaptive domains with the rectangular initial condition. Solutions in the adaptive domains are similar to the solution in the entire domain up to $K = 100$. As shown in Figs. 7a and b, it seems reasonable to adopt $K = 100$ for efficient and accurate computation.

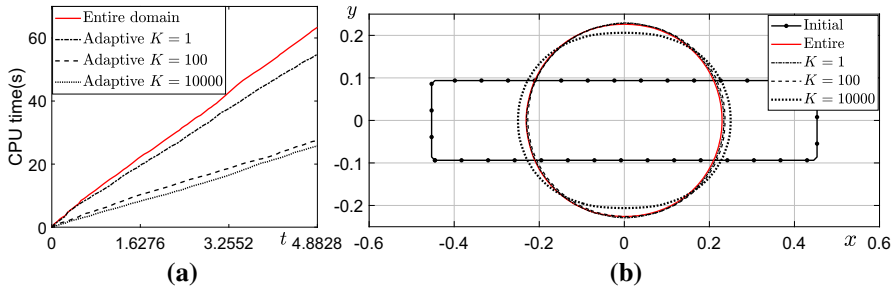


Fig. 7 On a computational domain $\Omega = (-1, 1) \times (-0.5, 0.5)$, for a rectangular initial condition, **a** CPU times and **b** contours of ϕ at zero for entire domain and adaptive domains with $K = 1, 100$, and 10000 . Here, $m = 4, h = 1/64, \Delta t = h^2$, and $t = 20000\Delta t$ are used

3.3 Three-Dimensional Space

We perform several computational experiments in 3D space. In 3D space, for stability and efficient computation, we use $\Delta t = 0.2h^2, m = 6, \xi = 0.5$, and $K = 100$. Figure 8 displays the temporal evolution of the cubic shape initial condition as follows:

$$\phi(x, y, z, 0) = \begin{cases} +1, & \text{if } -0.5 < x < 0.5, \quad -0.5 < y < 0.5, \quad -0.5 < z < 0.5, \\ -1, & \text{otherwise.} \end{cases}$$

To examine the efficiency of adaptive narrow-domain, a shape with irregularity is considered as the initial condition as shown in Fig. 9. In the case of the shape of Fig. 9, higher efficiencies can be obtained when using the adaptive narrow-band domain, compared to the case of solving the problems on the entire domain. Let us define the 3D discrete energy functional in the discretized space domain Ω_h as

$$\mathcal{E}^h(\phi^n) := \sum_{i=1}^{N_x} \sum_{j=1}^{N_y} \sum_{k=1}^{N_z} \left(F(\phi_{ijk}^n) + \frac{\epsilon^2}{2} |\nabla_h \phi_{ijk}^n|^2 \right) h^3, \tag{21}$$

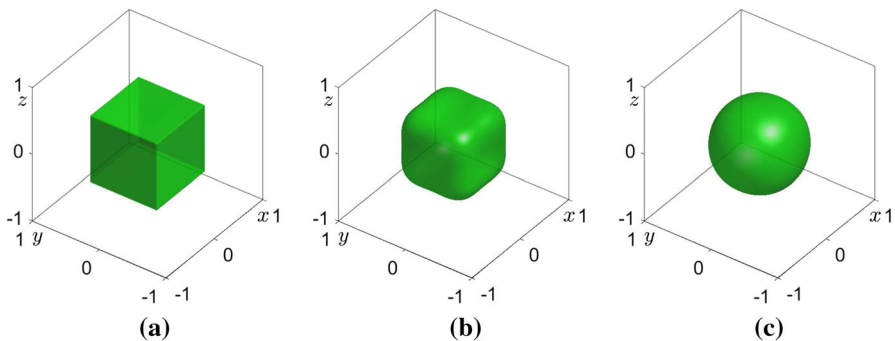


Fig. 8 Temporal evolution isosurface of ϕ at zero level with cube initial condition in 3D space. **a-c** are snapshots of solution for adaptive domain at $t = 0, t = 400\Delta t$, and $t = 3000\Delta t$, respectively

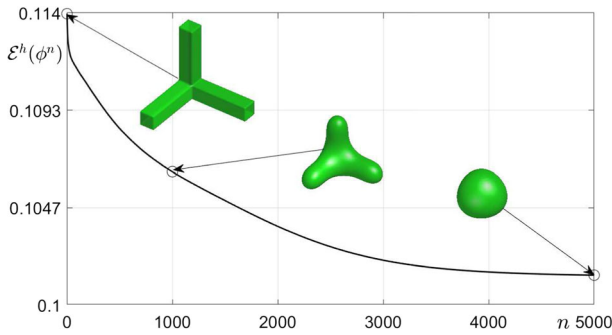


Fig. 9 Temporal evolution of the discrete free energy functional and dynamics with respect to the number of time iterations. Here, the solid line represents the energy curve, open circles represent the specific moments when $t = 0$, $t = 1000\Delta t$, and $t = 5000\Delta t$. From left to right, the figures inserted into the graph are snapshots of the zero level isosurface of solution ϕ with the irregular initial condition

where

$$\nabla_h \phi_{ijk}^n = \left(\frac{\phi_{i+1,jk}^n - \phi_{ijk}^n}{h}, \frac{\phi_{i,j+1,k}^n - \phi_{ijk}^n}{h}, \frac{\phi_{ij,k+1}^n - \phi_{ijk}^n}{h} \right). \tag{22}$$

In Fig. 9, the graph shows the temporal evolution of discrete free energy from $t = 0$ to $t = 5000\Delta t$ and the figures are snapshots of the zero level isosurface of ϕ with the irregular initial condition. We confirm that the discrete free energy functional decreases monotonically as time goes on.

Then, we investigate the robustness of the adaptive narrow-band domain for a shape with complex interface in 3D space. We consider ‘Genus 6 3D surface’ (Ceh Jan) as an initial condition, where the inside of the surface is 1 and the outside is -1, as shown in Fig. 10a. Figure 10a–d shows the temporal evolution of isosurface of ϕ at zero level with Genus 6 shape. As shown in Fig. 10, it can be seen that the adaptive narrow-band domain operates well for the CH equation for shapes with complex interfaces such as Genus 6 3D surface.

To validate the adaptive procedure for disjoint drops in 3D space, we consider the four separate drops, (see, e.g., Cheng et al. (2018)) consisting of three ellipsoids and one sphere. The initial condition is given as

$$\begin{aligned} \phi(x, y, z, 0) = & \tanh \left(\frac{\frac{\pi}{12} - \sqrt{0.25(x + \frac{\pi}{14})^2 + (y - \frac{\pi}{11})^2 + (z + \frac{\pi}{11})^2}}{\sqrt{2}\epsilon} \right) \\ & + \tanh \left(\frac{\frac{\pi}{12} - \sqrt{0.5(x - \frac{\pi}{10})^2 + (y + \frac{\pi}{13})^2 + (z + \frac{\pi}{11})^2}}{\sqrt{2}\epsilon} \right) \\ & + \tanh \left(\frac{\frac{\pi}{14} - \sqrt{(x + \frac{\pi}{10})^2 + (y + \frac{\pi}{12})^2 + (z + \frac{\pi}{11})^2}}{\sqrt{2}\epsilon} \right) \end{aligned}$$

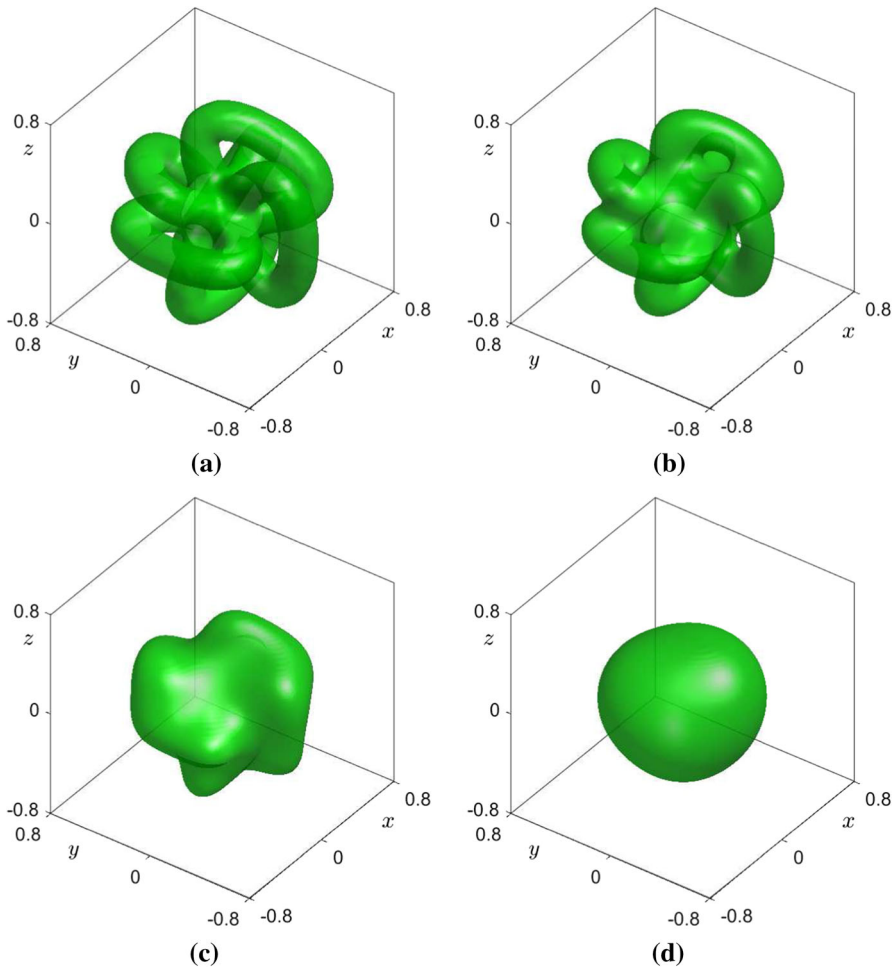


Fig. 10 Temporal evolution of isosurface of ϕ at zero level with Genus 6 shape for initial condition. **a–d** are snapshot of solution for the adaptive domain at $t = 0, t = 400\Delta t, t = 800\Delta t,$ and $t = 3000\Delta t,$ respectively

$$+ \tanh \left(\frac{\frac{\pi}{10} - \sqrt{x^2 + 0.2y^2 + (z - \frac{\pi}{10})^2}}{\sqrt{2}\epsilon} \right) + 3.$$

The isosurface of initial condition at $\phi = 0$ is illustrated in Fig. 11a. From the results in Fig. 11, four disjoint drops merge and eventually evolve into a sphere. The solution obtained by the proposed explicit adaptive method follows the dynamics of the CH equation well even if it is initially irregular or separated.

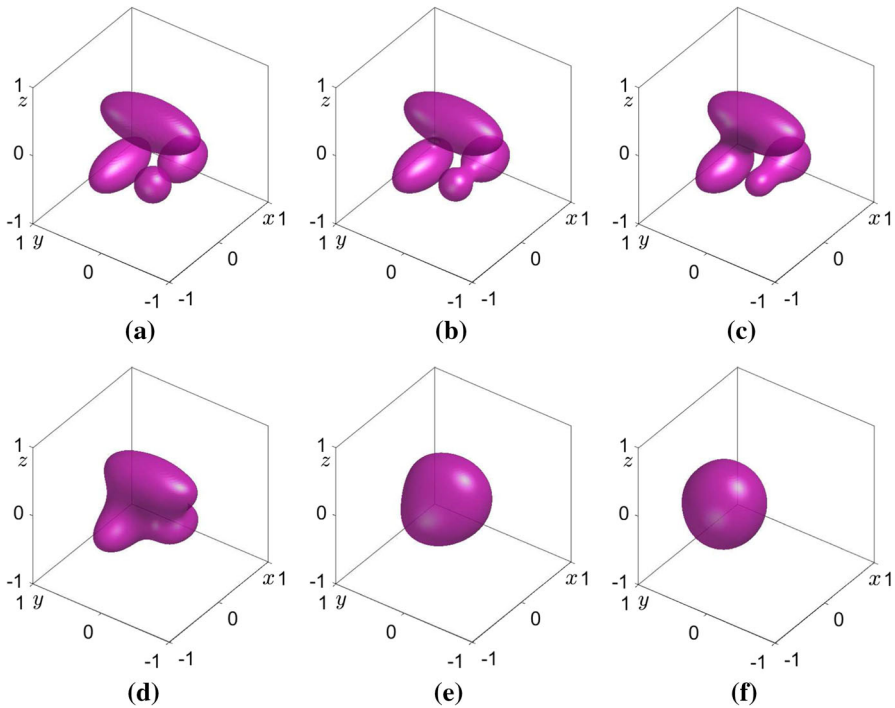


Fig. 11 a–f Snapshots of the isosurface of numerical solution ϕ at zero level with initially four drops, using the adaptive domain with $\Delta t = 4000h^4$ at $t = 0, t = 100\Delta t, t = 300\Delta t, t = 800\Delta t, t = 3000\Delta t,$ and $t = 50000\Delta t,$ respectively

4 Discussion and Conclusion

In this section, we discuss a relation between the interface layer parameter ϵ and the gradient criterion ξ . Then, we draw conclusions of this paper. An equilibrium profile is $\psi(x) = \tanh(x/(\sqrt{2}\epsilon))$ on the infinite domain, where the phase-field varies from -0.9 to 0.9 at a distance of about $2\sqrt{2} \tanh(0.9)$. Therefore, we use Eq. (17) for a transition layer width of approximately lh . We differentiate the equilibrium solution $\psi(x)$ to define the gradient criterion value ξ .

$$\psi'(x) = \frac{\text{sech}^2(x/(\sqrt{2}\epsilon))}{\sqrt{2}\epsilon}.$$

Thus, we define the relation between ξ and ϵ_l as follows:

$$\xi(\epsilon) = \left| \psi' \left(\sqrt{2}\epsilon \tanh^{-1}(0.995) \right) \right|, \tag{23}$$

which implies that our algorithm is set to recognize the transition layer more accurately. When $\epsilon = \epsilon_4$, using the relation (23), $\xi(\epsilon_4) \approx 0.4699$. In our previous numerical tests, we use $\xi = 0.5$ for simplicity.

In this paper, we presented an explicit adaptive FDM for the CH equation which describes the process of phase separation. To numerically solve the CH equation fast and efficiently, we used the FDM and time-adaptive narrow-band domain. For the adaptive grid, we define a narrow-band domain including the interfacial transition layer of the phase field and solve the numerical scheme on the narrow-band domain which is computed using undivided finite difference. We used the alternating direction explicit method. To make the scheme conservative, we apply a mass correction algorithm after each temporal iteration step. To demonstrate the superior performance of the proposed method, we presented 2D and 3D numerical experiments and compared them with those of the other previous methods. There exist several interesting future extensions of the proposed adaptive approach of the CH equation to other phase field models such as two-phase flows (Guo et al. 2022), multiphase tumor growth (Chen et al. 2014), topology optimization (Bartels et al. 2021; Yu et al. 2021), N -component CH system (Li et al. 2016b), N -component fluid flows (Kim 2009; Xia et al. 2022), curve and surface smoothing (Choi et al. 2017), and dendritic crystal growth (Zhang et al. 2019).

Acknowledgements The first author (S. Ham) was supported by the National Research Foundation (NRF), Korea, under project BK21 FOUR. Y.B. Li is supported by the Fundamental Research Funds for the Central Universities (No.XTR042019005). The corresponding author (J.S. Kim) was supported by Korea University Grant. The authors are grateful to the reviewers for their suggestions and comments on the revision of this article.

Availability of Data and Materials Data will be made available on reasonable request.

Declarations

Conflict of interest The authors declare that they have no conflict of interests.

References

- Ainsworth, M., Mao, Z.: Well-posedness of the Cahn-Hilliard equation with fractional free energy and its Fourier Galerkin approximation. *Chaos Solitons Fract.* **102**, 264–273 (2017)
- Banas, L.U., Nürnberg, R.: Adaptive finite element methods for Cahn-Hilliard equations. *J. Comput. Appl. Math.* **218**(1), 2–11 (2008)
- Bartels, A., Patrick, K., Jörn, M.: Cahn-Hilliard phase field theory coupled to mechanics: fundamentals, numerical implementation and application to topology optimization. *Comput. Meth. Appl. Mech. Eng.* **383**, 113918 (2021)
- Benesová, B., Melcher, C., Süli, E.: An implicit midpoint spectral approximation of nonlocal Cahn-Hilliard equations. *SIAM J. Numer. Anal.* **52**(3), 1466–1496 (2014)
- Berger, M.J., Colella, P.: Local adaptive mesh refinement for shock hydrodynamics. *J. Comput. Phys.* **82**(1), 64–84 (1989)
- Berger, M.J., Olinger, J.: Adaptive mesh refinement for hyperbolic partial differential equations. *J. Comput. Phys.* **53**, 484–512 (1984)
- Bosch, J., Stoll, M., Benner, P.: Fast solution of Cahn-Hilliard variational inequalities using implicit time discretization and finite elements. *J. Comput. Phys.* **262**, 38–57 (2014)
- Cahn, J.W., Hilliard, J.E.: Free energy of a non-uniform system I. Interfacial free energy. *J. Chem. Phys.* **28**(2), 258–267 (1958)
- Ceniceros, H.D., Rom, A.M.: A nonstiff, adaptive mesh refinement-based method for the Cahn-Hilliard equation. *J. Comput. Phys.* **225**(2), 1849–1862 (2007)

- Ceh Jan, Genus 6 3D surface, Craftsmanspace. <https://www.craftsmanspace.com/free-3d-models/genus-6-3d-surface.html>
- Cheng, K., Qiao, Z., Wang, C.: third order exponential time differencing numerical scheme for no-slope-selection epitaxial thin film model with energy stability. *J. Sci. Comput.* **81**(1), 154–185 (2019)
- Cheng, Q., Shen, J.: Multiple scalar auxiliary variable (MSAV) approach and its application to the phase-field vesicle membrane model. *SIAM J. Sci. Comput.* **40**(6), A3982–A4006 (2018)
- Chen, W., Conde, S., Wang, C., Wang, X., Wise, S.M.: A linear energy stable scheme for a thin film model without slope selection. *J. Sci. Comput.* **52**(3), 546–562 (2012)
- Chen, W., Li, W., Luo, Z., Wang, C., Wang, X.: A stabilized second order exponential time differencing multistep method for thin film growth model without slope selection. *ESAIM-Math. Model. Numer. Anal.* **54**(3), 727–750 (2020)
- Chen, W., Wang, C., Wang, X., Wise, S.M.: Positivity-preserving, energy stable numerical schemes for the Cahn-Hilliard equation with logarithmic potential. *J. Comput. Phys.* **X 3**, 100031 (2019)
- Chen, Y., Shen, J.: Efficient, adaptive energy stable schemes for the incompressible Cahn-Hilliard Navier-Stokes phase-field models. *J. Comput. Phys.* **308**, 40–56 (2016)
- Chen, Y., Lowengrub, J., Shen, J., Wang, C., Wise, S.: Efficient energy stable schemes for isotropic and strongly anisotropic Cahn-Hilliard systems with the Willmore regularization. *J. Comput. Phys.* **365**, 56–73 (2018)
- Chen, Y., Wise, S.M., Shenoy, V.B., Lowengrub, J.S.: A stable scheme for a nonlinear, multiphase tumor growth model with an elastic membrane. *Int. J. Numer. Meth. Biomed.* **30**(7), 726–754 (2014)
- Choi, Y., Jeong, D., Kim, J.: Curve and surface smoothing using a modified Cahn-Hilliard equation. *Math. Probl. Eng.* **2017**, (2017)
- Dohnal, T., Uecker, H.: Bifurcation of nonlinear Bloch waves from the spectrum in the Gross-Pitaevskii equation. *J. Nonlinear Sci.* **26**(3), 581–618 (2016)
- Dong, L., Wang, C., Zhang, H., Zhang, Z.: A Positivity-Preserving Second-Order BDF Scheme for the Cahn-Hilliard Equation with Variable Interfacial Parameters. *Commun. Comput. Phys.* **28**(3), 967–998 (2020)
- Feng, W., Guo, Z., Lowengrub, J.S., Wise, S.M.: A mass-conservative adaptive FAS multigrid solver for cell-centered finite difference methods on block-structured, locally-cartesian grids. *J. Comput. Phys.* **352**, 463–497 (2018)
- Feng, Y., Feng, Y., Iyer, G., Thiffeault, J.L.: Phase separation in the advective Cahn-Hilliard equation. *J. Nonlinear Sci.* **30**(6), 2821–2845 (2020)
- Fu, G., Han, D.: A linear second-order in time unconditionally energy stable finite element scheme for a Cahn-Hilliard phase-field model for two-phase incompressible flow of variable densities. *Comput. Meth. Appl. Mech. Eng.* **387**, 114186 (2021)
- Grant, C.P.: Spinodal decomposition for the Cahn-Hilliard equation. *Commun. Partial Differ. Equ.* **18**(3–4), 453–490 (1993)
- Grave, M., Coutinho, A.L.: Adaptive mesh refinement and coarsening for diffusion-reaction epidemiological models. *Comput. Mech.* **67**(4), 1177–1199 (2021)
- Guo, J., Wang, C., Wise, S.M., Yue, X.: An H^2 convergence of a second-order convex-splitting, finite difference scheme for the three-dimensional Cahn-Hilliard equation. *Commun. Math. Sci.* **14**(2), 489–515 (2016)
- Guo, J., Wang, C., Wise, S.M., Yue, X.: An improved error analysis for a second-order numerical scheme for the Cahn-Hilliard equation. *J. Comput. Appl. Math.* **388**, 113300 (2021)
- Guo, Z., Cheng, Q., Lin, P., Liu, C., Lowengrub, J.: Second order approximation for a quasi-incompressible Navier-Stokes Cahn-Hilliard system of two-phase flows with variable density. *J. Comput. Phys.* **448**, 110727 (2022)
- Hao, Y., Huang, Q., Wang, C.: A third order BDF energy stable linear scheme for the no-slope-selection thin film model. *Commun. Comput. Phys.* **29**(3), 905–929 (2021)
- Jeong, D., Li, Y., Lee, C., Yang, J., Kim, J.: A conservative numerical method for the Cahn-Hilliard equation with generalized mobilities on curved surfaces in three-dimensional space. *Commun. Comput. Phys.* **27**(2), 412–430 (2020)
- Jeong, D., Li, Y., Choi, Y., Lee, C., Yang, J., Kim, J.: A practical adaptive grid method for the Allen-Cahn equation. *Phys. A* **573**, 125975 (2021)
- Jung, M., Yoo, J.: Phase field-based topology optimization of metallic structures for microwave applications using adaptive mesh refinement. *Struct. Multidiscip. Optim.* **63**(6), 2685–2704 (2021)

- Kay, D., Welford, R.: A multigrid finite element solver for the Cahn-Hilliard equation. *J. Comput. Phys.* **212**(1), 288–304 (2006)
- Kim, J.: A generalized continuous surface tension force formulation for phase-field models for multi-component immiscible fluid flows. *Comput. Meth. Appl. Mech. Eng.* **198**(37–40), 3105–3112 (2009)
- Koliesnikova, D., Ramière, I., Lebon, F.: A unified framework for the computational comparison of adaptive mesh refinement strategies for all-quadrilateral and all-hexahedral meshes: Locally adaptive multigrid methods versus h-adaptive methods. *J. Comput. Phys.* **437**, 110310 (2021)
- Lee, C., Jeong, D., Shin, J., Li, Y., Kim, J.: A fourth-order spatial accurate and practically stable compact scheme for the Cahn-Hilliard equation. *Phys. A* **409**, 17–28 (2014)
- Li, D., Qiao, Z.: On second order semi-implicit Fourier spectral methods for 2D Cahn-Hilliard equations. *J. Sci. Comput.* **70**(1), 301–341 (2017)
- Li, D., Qiao, Z., Tang, T.: Characterizing the stabilization size for semi-implicit Fourier-spectral method to phase field equations. *SIAM J. Numer. Anal.* **54**(3), 1653–1681 (2016)
- Li, H., Yamada, T., Jolivet, P., Furuta, K., Kondoh, T., Izui, K., Nishiwaki, S.: Full-scale 3D structural topology optimization using adaptive mesh refinement based on the level-set method. *Finite Elem. Anal. Des.* **194**, 103561 (2021)
- Li, W., Chen, W., Wang, C., Yan, Y., He, R.: A second order energy stable linear scheme for a thin film model without slope selection. *J. Sci. Comput.* **76**(3), 1905–1937 (2018)
- Li, X., Qiao, Z., Wang, C.: Convergence analysis for a stabilized linear semi-implicit numerical scheme for the nonlocal Cahn-Hilliard equation. *Math. Comput.* **90**(327), 171–188 (2021)
- Li, Y., Choi, J.I., Kim, J.: A phase-field fluid modeling and computation with interfacial profile correction term. *Commun. Nonlinear Sci. Numer. Simul.* **30**, 84–100 (2016)
- Li, Y., Choi, J.I., Kim, J.: Multi-component Cahn-Hilliard system with different boundary conditions in complex domains. *J. Comput. Phys.* **323**, 1–16 (2016)
- Li, Y., Choi, Y., Kim, J.: Computationally efficient adaptive time step method for the Cahn-Hilliard equation. *Comput. Math. Appl.* **73**(8), 1855–1864 (2017)
- Li, Y., Jeong, D., Kim, J.: Adaptive mesh refinement for simulation of thin film flows. *Meccanica* **49**(1), 239–252 (2014)
- Li, Y., Kim, J.: Phase-field simulations of crystal growth with adaptive mesh refinement. *Int. J. Heat Mass Transf.* **55**, 7926–7932 (2012)
- Li, Y., Kim, J.: An efficient and stable compact fourth-order finite difference scheme for the phase field crystal equation. *Comput. Meth. Appl. Mech. Eng.* **319**, 194–216 (2017)
- Li, Y., Lee, H.G., Xia, B., Kim, J.: A compact fourth-order finite difference scheme for the three-dimensional Cahn-Hilliard equation. *Comput. Phys. Commun.* **200**, 108–116 (2016)
- Meng, X., Qiao, Z., Wang, C., Zhang, Z.: Artificial regularization parameter analysis for the no-slope-selection epitaxial thin film model. *CSIAM Trans. Appl. Math* **1**(3), 441–462 (2020)
- Mohammadi, V., Dehghan, M.: Simulation of the phase field Cahn-Hilliard and tumor growth models via a numerical scheme: element-free Galerkin method. *Comput. Meth. Appl. Mech. Eng.* **345**, 919–950 (2019)
- Sun, P., Russell, R.D., Xu, J.: A new adaptive local mesh refinement algorithm and its application on fourth order thin film flow problem. *J. Comput. Phys.* **224**(2), 1021–1048 (2007)
- Stogner, R.H., Carey, G.F., Murray, B.T.: Approximation of Cahn-Hilliard diffuse interface models using parallel adaptive mesh refinement and coarsening with C^1 elements. *Int. J. Numer. Meth. Eng.* **76**, 636–661 (2008)
- Theljani, A., Houichet, H., Mohamed, A.: An adaptive Cahn-Hilliard equation for enhanced edges in binary image inpainting. *J. Algorithms Comput. Technol.* **14**, 1748302620941430 (2020)
- Wise, S., Kim, J., Lowengrub, J.: Solving the regularized, strongly anisotropic Cahn-Hilliard equation by an adaptive nonlinear multigrid method. *J. Comput. Phys.* **226**(1), 414–446 (2007)
- Wise, S.M., Lowengrub, J.S., Cristini, V.: An adaptive multigrid algorithm for simulating solid tumor growth using mixture models. *Math. Comput. Model.* **53**(1–2), 1–20 (2011)
- Xia, Q., Kim, J., Yibao, L.: Modeling and simulation of multi-component immiscible flows based on a modified Cahn-Hilliard equation. *Eur. J. Mech. B-Fluids* **95**, 194–204 (2022)
- Xu, J., Li, Y., Wu, S., Bousquet, A.: On the stability and accuracy of partially and fully implicit schemes for phase field modeling. *Comput. Meth. Appl. Mech. Eng.* **345**, 826–853 (2019)
- Yang, J., Li, Y., Lee, C., Lee, H.G., Kwak, S., Hwang, Y., Xin, X., Kim, J.: An explicit conservative Saul'yev scheme for the Cahn-Hilliard equation. *Int. J. Mech. Sci.* **217**, 106985 (2022)

- Yu, Q., Wang, K., Xia, B., Li, Y.: First and second order unconditionally energy stable schemes for topology optimization based on phase field method. *Appl. Math. Comput.* **405**, 126267 (2021)
- Zhang, J., Chen, C., Yang, X.: A novel decoupled and stable scheme for an anisotropic phase-field dendritic crystal growth model. *Appl. Math. Lett.* **95**, 122–129 (2019)
- Zhai, S., Weng, Z., Yang, Y.: A high order operator splitting method based on spectral deferred correction for the nonlocal viscous Cahn-Hilliard equation. *J. Comput. Phys.* **446**, 110636 (2021)
- Zhou, S., Xie, Y.M.: Numerical simulation of three-dimensional multicomponent Cahn-Hilliard systems. *Int. J. Mech. Sci.* **198**, 106349 (2021)
- Zhu, J., Chen, L.Q., Shen, J., Tikare, V.: Coarsening kinetics from a variable-mobility Cahn-Hilliard equation: application of a semi-implicit Fourier spectral method. *Phys. Rev. E* **60**, 3564–3572 (1999)

Publisher's Note Springer Nature remains neutral with regard to jurisdictional claims in published maps and institutional affiliations.

Springer Nature or its licensor holds exclusive rights to this article under a publishing agreement with the author(s) or other rightsholder(s); author self-archiving of the accepted manuscript version of this article is solely governed by the terms of such publishing agreement and applicable law.